Frontiers in Bioscience Landmark

Front. Biosci. (Landmark Ed) **2026**; 31(6): 50432
https://doi.org/10.31083/FBL50432

Original Research

The Interaction Between Iron Overload and Lead Exposure on Bone Metabolism

Yongjie Yang[1,2], Tianbao Gong[1,2], Haitao Ma[1,2], Liyin Liu[3], Defu Yu[2], Tao Chen[1,2,4,*]

[1]Graduate School, Bengbu Medical University, 233030 Bengbu, Anhui, China
[2]Department of Orthopedic Surgery, Anhui No. 2 Provincial People's Hospital, 230041 Hefei, Anhui, China
[3]School of Basic Medical Sciences, Anhui Medical University, 230032 Hefei, Anhui, China
[4]Now with Anhui Provincial Institute of Occupational Disease Control, 230041 Hefei, Anhui, China
*Correspondence: seygkchentao@163.com (Tao Chen)
Academic Editor: Elisa Belluzzi
Submitted: 27 January 2026 Revised: 14 April 2026 Accepted: 20 April 2026 Published: 15 June 2026

Abstract

Background: Osteoporosis (OP) is a common metabolic bone disease characterized by chronic bone loss and structural deterioration of bone tissue, and it is closely associated with environmental exposure to heavy metals. Although lead (Pb) and iron (Fe) are known to affect bone metabolism, the impact of iron overload under fixed lead exposure, along with the underlying metabolic mechanisms, remains unclear. This study aimed to investigate the effects of combined iron and lead exposure on bone mineral homeostasis and metabolic remodeling. **Methods**: Male C57BL/6 mice were exposed for 8 weeks to lead acetate (50 mg/kg) in combination with either low-dose (100 mg/kg) or high-dose (300 mg/kg) iron dextran. Metal accumulation in femoral tissue was quantified using inductively coupled plasma mass spectrometer (ICP-MS). Bone microarchitecture was evaluated using microcomputed tomography (micro-CT). Bone-specific untargeted metabolomics and Kyoto Encyclopedia of Genes and Genomes (KEGG) pathway analyses were performed to assess metabolic alterations. **Results**: Iron overload did not significantly affect lead accumulation but disrupted mineral balance in a dose-dependent manner, reducing levels of calcium, zinc, magnesium, and vanadium. Micro-CT analysis revealed significant alterations in bone microarchitecture. Metabolomic analysis identified 297 altered metabolites, primarily involved in amino acid, lipid, and nucleotide metabolism, as well as mineral absorption. KEGG pathway analysis revealed disturbances in amino acid biosynthesis, aminoacyl-tRNA biosynthesis, ATP-binding cassette (ABC) transporters, protein digestion and absorption, and mineral absorption, with distinct profiles observed between different iron doses. **Conclusions**: Iron overload is associated with further alterations in bone metabolic homeostasis under fixed lead exposure, as evidenced by structural deterioration, disruption of trace element homeostasis, and extensive metabolic reprogramming in bone tissue.

Keywords: osteoporosis; iron; lead; metabolomics; bone metabolism

1. Introduction

Osteoporosis (OP) is a metabolic bone disorder characterized by reduced bone mass and deterioration of bone microarchitecture, and exposure to heavy metals has been identified as a major risk factor [1,2,3,4]. Lead, a widespread environmental contaminant, affects not only the nervous, hematopoietic, and renal systems but is also strongly associated with bone health [5,6]. Lead (Pb) exhibits a strong affinity for bone tissue and may contribute to the development of osteoporosis by suppressing osteogenesis, enhancing osteoclast activity, and disrupting mineralization [7]. Iron (Fe), an essential trace element in humans, plays a critical role in various physiological processes, including oxygen transport, energy metabolism, and cell growth [8]. However, disturbances in iron metabolism, such as iron overload, have been linked to several health problems, including liver, cardiac, and bone diseases [9,10]. Recent studies suggest that iron overload may disturb the balance between bone formation and resorption by inducing oxidative stress, inflammatory responses, and cell death, thereby contributing to the onset and progression of osteoporosis [11,12].

Iron and lead share common transport proteins, such as divalent metal transporter 1 (DMT1), suggesting a potential competitive or synergistic relationship between these two elements in the body [13]. However, considerable debate remains regarding how iron status influences the tissue distribution and toxicity of lead [14,15], particularly with respect to their interactions in bone tissue, which have not yet been fully validated experimentally. With advances in systems biology, metabolomics has emerged as a powerful approach for investigating disease-related molecular phenotypes, as it provides a direct measure of changes in end metabolites [16]. In contrast to proteomics and transcriptomics, which often reflect potential functional changes, metabolomics directly captures the end products of small-molecule metabolism [17]. This approach provides a more accurate representation of physiological states and pathological processes, offering significant advantages for the study of bone metabolism. Compared with blood or other

tissues, bone tissue metabolomics can more clearly reveal key alterations in mineral homeostasis, amino acid metabolism, lipid turnover, and energy metabolism within the bone matrix [18,19]. It serves as a direct indicator of metabolic responses in osteocytes during exposure, injury, and repair [20,21]. Therefore, bone-focused metabolomic studies represent a highly targeted and effective strategy for investigating environmentally induced bone metabolic disorders.

Our research group previously found that co-exposure to low levels of lead and iron altered bone damage in mice [22]. To further investigate how combined exposure to these two metals affects bone metabolism, we administered different doses of iron while maintaining a constant level of lead exposure. Using a controlled-variable design, we investigated the effects of iron and lead on bone metabolism and metabolite profiles, thereby further clarifying their roles in the onset and progression of bone metabolic disorders. This study not only improves our understanding of how heavy metal interactions affect skeletal health but also provides new insights into the prevention and treatment of environmentally induced osteoporosis.

2. Materials and Methods

2.1 Animals

Male C57BL/6 mice (8 weeks old, 18–22 g) were obtained from Henan Skyboss Biotechnology Co., Ltd. (Certification No. SCXK 2020-0005, Henan, China). The animals were housed in a specific pathogen-free facility at Anhui Medical University (Anhui, China) under controlled environmental conditions (22–25 °C and 40–60% relative humidity) with a 12 h light/dark cycle and free access to standard chow and water. The animals were provided with ultrapure water free of detectable lead and iron contamination, as well as standard laboratory chow containing no added lead and only trace amounts of iron required for normal nutrition. After a 1-week acclimation period, a total of 24 mice were included in the study. All animal experimental procedures were reviewed and approved by the Ethics Committee of Anhui Medical University (Approval No. 2024-2251).

2.2 Animal Experiments

Following acclimation, 24 mice were randomly assigned to four experimental groups: a control group (Control), a lead-exposed group (Pb50), a low-dose iron plus lead group (Fe100_Pb50), and a high-dose iron plus lead group (Fe300_Pb50). Mice were housed in separate cages (n = 6 per group). Animals in the treatment groups received iron dextran by intraperitoneal injection once weekly (100 mg/kg for the low-dose group and 300 mg/kg for the high-dose group) and lead acetate by oral gavage (50 mg/kg) three times per week. For all administrations, the dosing volume was normalized to body weight (0.01 mL/g) [22].

Body weight was recorded daily throughout the 8-week exposure period. No abnormal mortality or severe treatment-related complications were observed. Humane endpoints were predefined as a body weight loss exceeding 20%, marked lethargy, or impaired access to food or water; none of these criteria were met during the study.

At the end of the exposure period, mice were fasted for 12 h before tissue collection. Anesthesia was induced by intraperitoneal injection of pentobarbital sodium (0.3%, 30 mg/kg). After a deep anesthetic state was confirmed, the animals were humanely euthanized by cervical dislocation in accordance with approved ethical standards. Subsequently, the skin and muscle tissues of the hind limbs were removed, and both femurs were collected. Femur samples from each group were collected and allocated for different analyses. Specifically, femurs from a subset of mice were fixed in 4% paraformaldehyde and used for ICP-MS and micro-CT analysis, whereas femurs from additional mice were stored at −80 °C for metabolomic analysis.

2.3 Measurement of Heavy Metal Levels in Bone Tissue

The left femur samples collected from each group of mice were ultrasonically cleaned to remove blood and residual tissue from the surface. After cleaning, the femur samples were cut into smaller pieces to improve the efficiency of metal extraction. The samples were then digested to remove organic components from the bone matrix, thereby ensuring accurate extraction of metal elements. Metal levels in mouse bone tissue were measured using an inductively coupled plasma mass spectrometer (ICP-MS 7800, Agilent, G8421A, USA). The resulting metal concentration data were subjected to subsequent statistical analysis.

2.4 Micro-CT Analysis of Mouse Femurs

Femur samples were fixed and scanned using a micro-CT system (Bruker, Ettlingen, Germany) under standardized conditions: 60 kV, 200 μA, 6.55 μm resolution, 205 ms exposure time, and 180° rotation. A calibration phantom was scanned under the same conditions. Three-dimensional reconstruction was performed using NRecon (Software version V1.7.4.2, Bruker, Germany). Quantitative analysis of the distal femoral trabecular region was then conducted using CTAn software. Bone parameters, including bone volume fraction (BV/TV), bone mineral density (BMD), trabecular number (Tb.N), and trabecular separation (Tb.Sp), were calculated for subsequent statistical analysis.

2.5 Metabolomic Analysis of Mouse Bone Tissue

Untargeted metabolomic analysis of bone tissue was performed by BGI Genomics (Shenzhen, China). Six femur samples were collected from each group. Upon receipt, each sample was renumbered. A 25 mg aliquot of each sample was transferred into a thick-walled centrifuge tube containing two small magnetic beads. A mixed internal standard solution containing stable isotope-labelled

standards (including d3-leucine and 13C9-phenylalanine) was then added, followed by 800 µL of pre-cooled extraction solvent consisting of methanol, acetonitrile, and water (2:2:1, v/v/v). The samples were homogenized using a tissue grinder (JXFSTPRP, Shanghai Jingxin, China) at 50 Hz for 5 min to ensure complete release of intracellular metabolites. The samples were then precipitated at −20 °C for 2 h and centrifuged at 25,000 ×g at 4 °C for 15 min. The supernatant from each sample was transferred to a new EP tube, and 600 µL was subjected to freeze-drying. The dried metabolites were reconstituted in 600 µL of 50% methanol. After repeated centrifugation, the supernatant was transferred to new EP tubes, and 10 µL from each sample was pooled to generate a mixed quality control (QC) sample for evaluating repeatability and stability throughout the analytical process.

Metabolite separation and identification were performed using an ultra-high-performance liquid chromatography tandem high-resolution mass spectrometry (UPLC-MS/MS) system. Mass spectrometric detection was performed using a Q Exactive HF mass spectrometer (Thermo Fisher Scientific, Waltham, MA, USA) to acquire both MS and MS/MS spectra. The mass scan range was set from m/z 70 to 1050, with a full-scan resolution of 120,000, an automatic gain control (AGC) target of 3×10^6, and a maximum injection time (IT) of 100 ms. The top three precursor ions were selected for fragmentation based on signal intensity, and MS/MS data were acquired at a resolution of 30,000, with an AGC target of 1×10^5 and a maximum IT of 50 ms. The stepped normalized collision energy (NCE) was set to 20, 40, and 60 eV. The electrospray ionization (ESI) source parameters were as follows: sheath gas flow rate, 40; auxiliary gas flow rate, 10; spray voltage, 3.80 kV in positive ion mode and 3.20 kV in negative ion mode. The capillary temperature was maintained at 320 °C, and the auxiliary gas heater temperature was set at 350 °C.

Raw mass spectrometry data were first imported into Compound Discoverer 3.3 (Thermo Fisher Scientific, USA) for peak extraction, alignment, and metabolite identification. Metabolic features with a relative standard deviation (RSD) >30% in QC samples were excluded to ensure data quality. Subsequently, multivariate statistical analyses, including principal component analysis (PCA) and orthogonal partial least squares discriminant analysis (OPLS-DA), were used to identify high-confidence differential metabolites (Variable Importance in Projection [VIP] $\geq$1, absolute $\log_2$-fold change ($|\log_2 FC|$) $\geq$1.5, and $p < 0.05$). Pathway enrichment analysis was then performed using the Kyoto Encyclopedia of Genes and Genomes (KEGG) to clarify the biological functions of these differential metabolites. Information on differential metabolites in the femurs of each mouse group was obtained through the Dr. Tom platform (https://biosys.bgi.com/), where additional analyses were also performed.

2.6 Statistical Analysis

Statistical analyses were performed using GraphPad Prism 10 (GraphPad Software, USA) and Origin (OriginLab, USA). All data are presented as the mean ± standard deviation (SD). Data normality and homogeneity of variance were assessed prior to parametric analyses. For comparisons between two groups, Student's *t*-test was used. For comparisons among multiple groups, one-way analysis of variance (ANOVA) followed by Tukey's post hoc test was applied. Linear regression analysis was conducted using Origin to evaluate the relationships between iron and other metal elements in bone tissue.

For correlation analyses, Pearson's correlation coefficient was used to assess linear relationships between metal concentrations, whereas Spearman's rank correlation analysis was used to evaluate correlations among differential metabolites. For metabolomics data, multivariate statistical analyses, including principal component analysis (PCA), partial least squares discriminant analysis (PLS-DA), and orthogonal partial least squares discriminant analysis (OPLS-DA), were performed to visualize group separation and identify differential metabolites. Model validity was evaluated by permutation testing to minimize the risk of overfitting.

Differential metabolites were identified based on Variable Importance in Projection (VIP) values $\geq$1, absolute $\log_2$-fold change ($|\log_2 FC|$) $\geq$1.5, and p values < 0.05. Statistical significance was defined as $p < 0.05$ for all analyses.

3. Results

3.1 The Effects of Combined Iron and Lead Exposure on Metal Elements in the Femur of Mice

3.1.1 Effects of Combined Iron–Lead Exposure on Lead Deposition, and Calcium Loss in Mice

To examine the effect of iron exposure on the distribution of metal elements in bone, metal concentrations in femurs from experimental groups were measured using ICP-MS. Iron levels in bone tissue differed significantly among the exposure groups. Compared with the Pb50 group, iron levels in the Fe100_Pb50 and Fe300_Pb50 groups were significantly increased in a dose-dependent manner (Fig. 1A). Lead concentrations in bone were then analyzed across the different groups (Fig. 1B). Lead levels in the Fe100_Pb50 and Fe300_Pb50 groups were lower than those in the Pb50 group; however, these differences were not statistically significant (ns). Calcium levels, a key element in bone metabolism, were subsequently measured (Fig. 1C). Compared with the Pb50 group, bone calcium levels in the Fe100_Pb50 and Fe300_Pb50 groups were significantly reduced. A significant difference was also observed between the Fe300_Pb50 and Fe100_Pb50 groups (*$p < 0.05$), indicating a dose-dependent decrease in calcium levels with increasing iron exposure. Linear regression analysis of iron with lead and calcium levels further supported these findings (**Supplementary Fig. 1**).

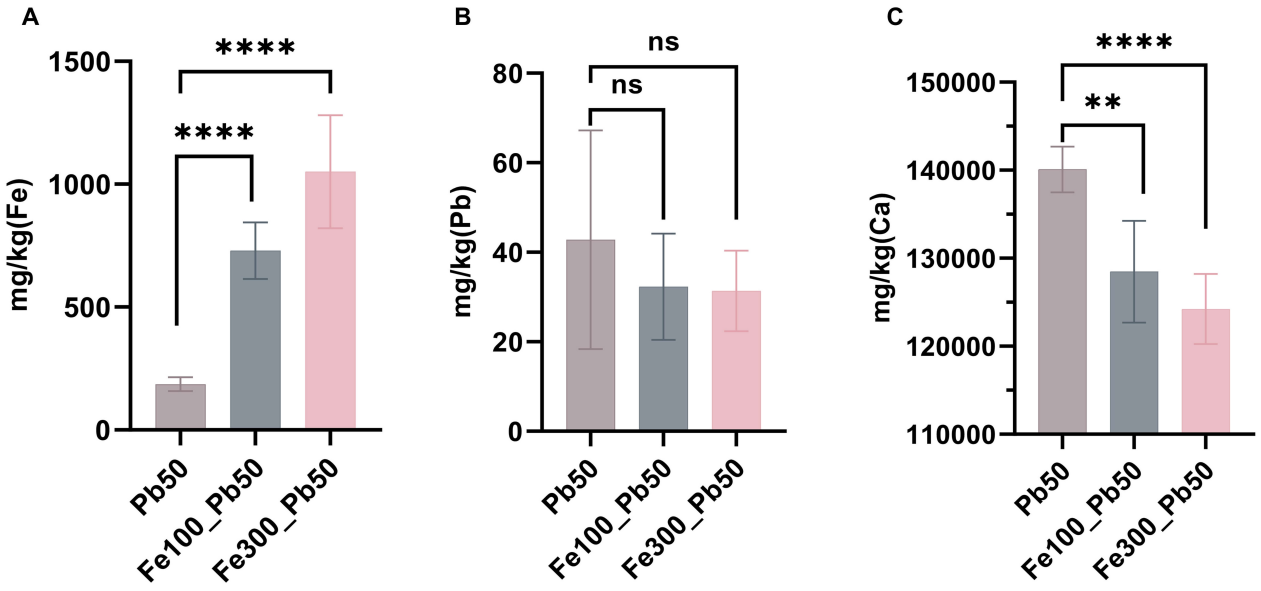

Fig. 1. Changes in iron, lead, and calcium levels in mouse femurs. (A) Iron levels in femurs from each group (Pb50, Fe100_Pb50, Fe300_Pb50). (B) Lead levels in femurs showed no significant differences among groups (ns). (C) Calcium levels in femurs differed significantly among groups (**$p < 0.01$; ****$p < 0.0001$). Data are presented as the mean ± standard deviation (SD).

3.1.2 Correlations Between Iron and Other Trace Metals Under Combined Metal Exposure

Trace elements are essential for bone metabolism and overall physiological homeostasis, maintaining a tightly regulated balance among themselves [23]. Abnormal accumulation or deficiency of a specific metal may disrupt the homeostasis of others, potentially through mechanisms such as competitive absorption, altered transporter affinity, or changes in tissue distribution [24,25]. To further investigate these interactions, we measured additional metal concentrations in mouse femurs and performed linear regression analyses of zinc (Zn), magnesium (Mg), and vanadium (V) against iron (Fe). Iron levels were negatively correlated with zinc concentrations, with regression analysis indicating a significant decrease in zinc as iron increased (Fig. 2A). A similar negative correlation was observed between iron and magnesium, with higher iron levels associated with lower magnesium concentrations (Fig. 2B). Iron also showed a negative correlation with vanadium, with regression analysis indicating that increased iron levels were significantly associated with reduced vanadium concentrations (Fig. 2C). All correlations were statistically significant, suggesting that iron overload may substantially influence the homeostasis of these trace elements.

3.2 Effects of Combined Iron and Lead Exposure on Mouse Femur Microarchitecture

To assess bone microarchitecture in mice, three-dimensional micro-CT reconstructions of femurs were generated. Compared with the control group, the experimental groups (Pb50, Fe100_Pb50, and Fe300_Pb50) exhibited marked alterations in bone microarchitecture (Fig. 3A–D). Quantitative analysis revealed that, in the Pb50 group, trabecular number (Tb.N) was significantly decreased, whereas bone mineral density (BMD), bone volume fraction (BV/TV), and trabecular separation (Tb.Sp) showed no significant changes. In contrast, under constant lead exposure, increasing iron doses showed a dose-related trend of reductions in BMD, BV/TV, and Tb.N (Fig. 3E–G), along with a significant increase in Tb.Sp (Fig. 3H). Based on these structural changes, we further investigated the effects of combined iron and lead exposure on bone metabolic homeostasis at the metabolomic level.

3.3 Identification of Differential Metabolites in Mouse Femurs, Correlation Analysis, and Pathway Enrichment Analysis

3.3.1 Identification of Differential Metabolites in Mouse Femurs

Untargeted metabolomics was performed to investigate metabolic alterations in bone tissue under varying levels of iron–lead co-exposure. A total of 8970 metabolites were detected. After excluding 6609 unannotated metabolites, 2361 annotated metabolites were retained, including 1320 and 1041 detected in positive and negative ion modes, respectively. Data quality was assessed using principal component analysis (PCA) and orthogonal partial least squares discriminant analysis (OPLS-DA). PCA score plots showed clear separation between groups (e.g., Fe100_Pb50 vs Pb50 and Fe300_Pb50 vs Pb50), with tight clustering and no evident outliers (Fig. 4A,B). The variance explained by the principal components (e.g., 16.229% and 18.523%) supported the observed group separation.

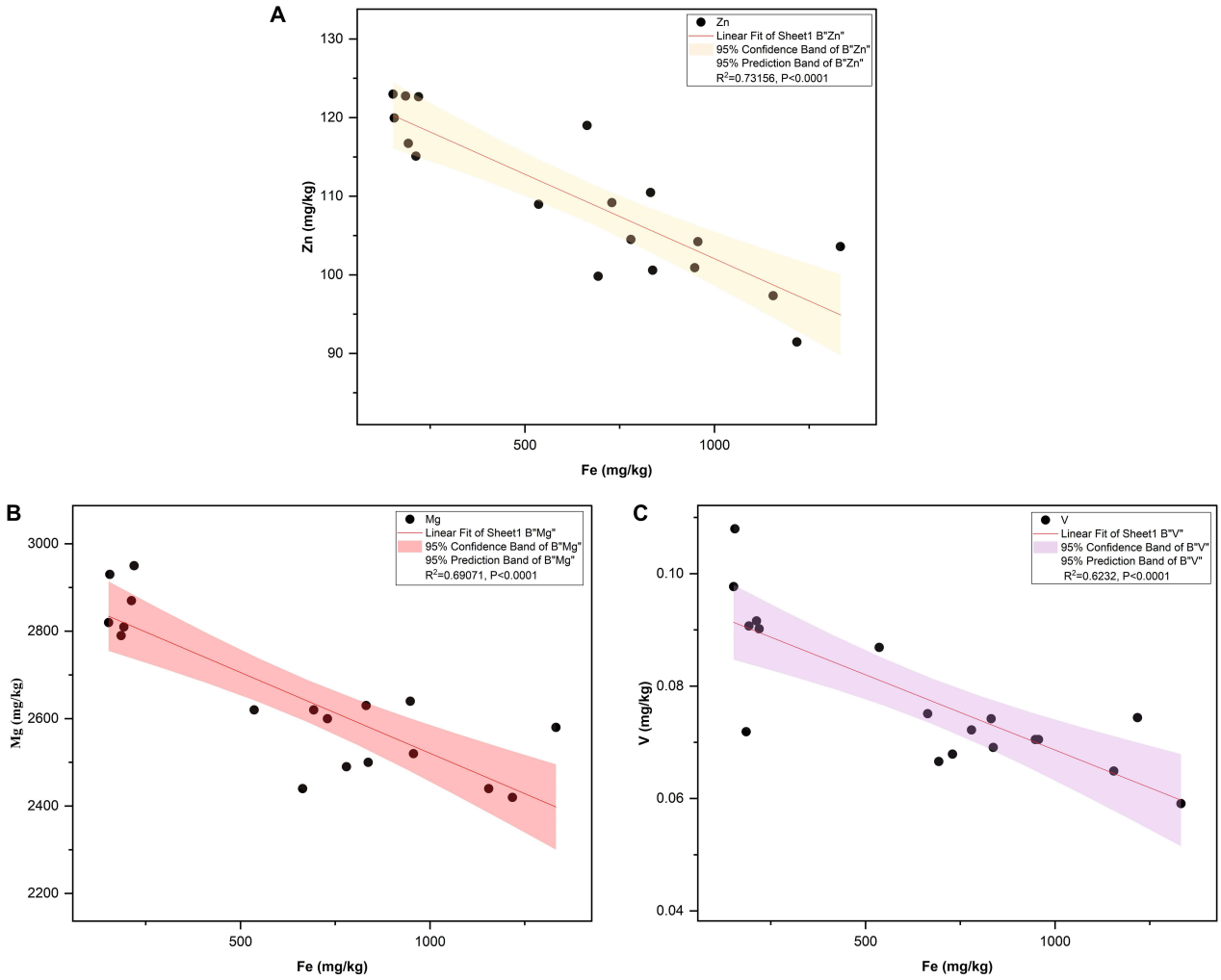

Fig. 2. Linear relationships between iron and trace metal concentrations. (A–C) Negative correlations between iron (Fe) and zinc (Zn), magnesium (Mg), and vanadium (V). Each panel shows the linear regression fit with 95% confidence and prediction intervals. All correlations were statistically significant ($p < 0.0001$), with R^2 values of 0.7316, 0.6907, and 0.6232, respectively, indicating strong explanatory power for the variability in the corresponding trace metal concentrations.

OPLS-DA score plots further confirmed clear separation between groups, with orthogonal component contributions (e.g., 11.2% and 11.8%) highlighting distinct metabolic profiles and no apparent batch effects (Fig. 4C,D). These results indicate high data quality and robust intergroup differences, supporting the reliability of subsequent analyses.

3.3.2 Identification of Differential Metabolites

Compared with the Pb50 group, substantial metabolic alterations were observed in bone tissue following iron exposure. A total of 297 differential metabolites were identified across the groups; all met the criteria of VIP $\geq$1, $|\log_2 FC| \geq 1.5$, and $p < 0.05$ and were subsequently used for downstream pathway enrichment analysis. In the Fe100_Pb50 vs Pb50 comparison, 66 differential metabolites were identified, including 35 upregulated and 31 downregulated metabolites. In the Fe300_Pb50 vs Pb50 comparison, 266 differential metabolites were identified, including 171 upregulated and 95 downregulated metabolites (Fig. 5A).

Venn diagram analysis revealed both shared and unique differential metabolites among the groups (Fig. 5B). Specifically, 31 metabolites were unique to the Fe100_Pb50 group (15 upregulated and 16 downregulated), whereas 231 metabolites were unique to the Fe300_Pb50 group (151 upregulated and 80 downregulated). A total of 35 metabolites were shared between the two groups (20 upregulated and 15 downregulated).

Volcano plots further demonstrated clear separation and significant metabolic alterations between the groups (Fig. 5C,D). The top 15 upregulated and downregulated metabolites were further analyzed and ranked based on fold change values. In the Fe100_Pb50 vs Pb50 comparison, the most significantly upregulated

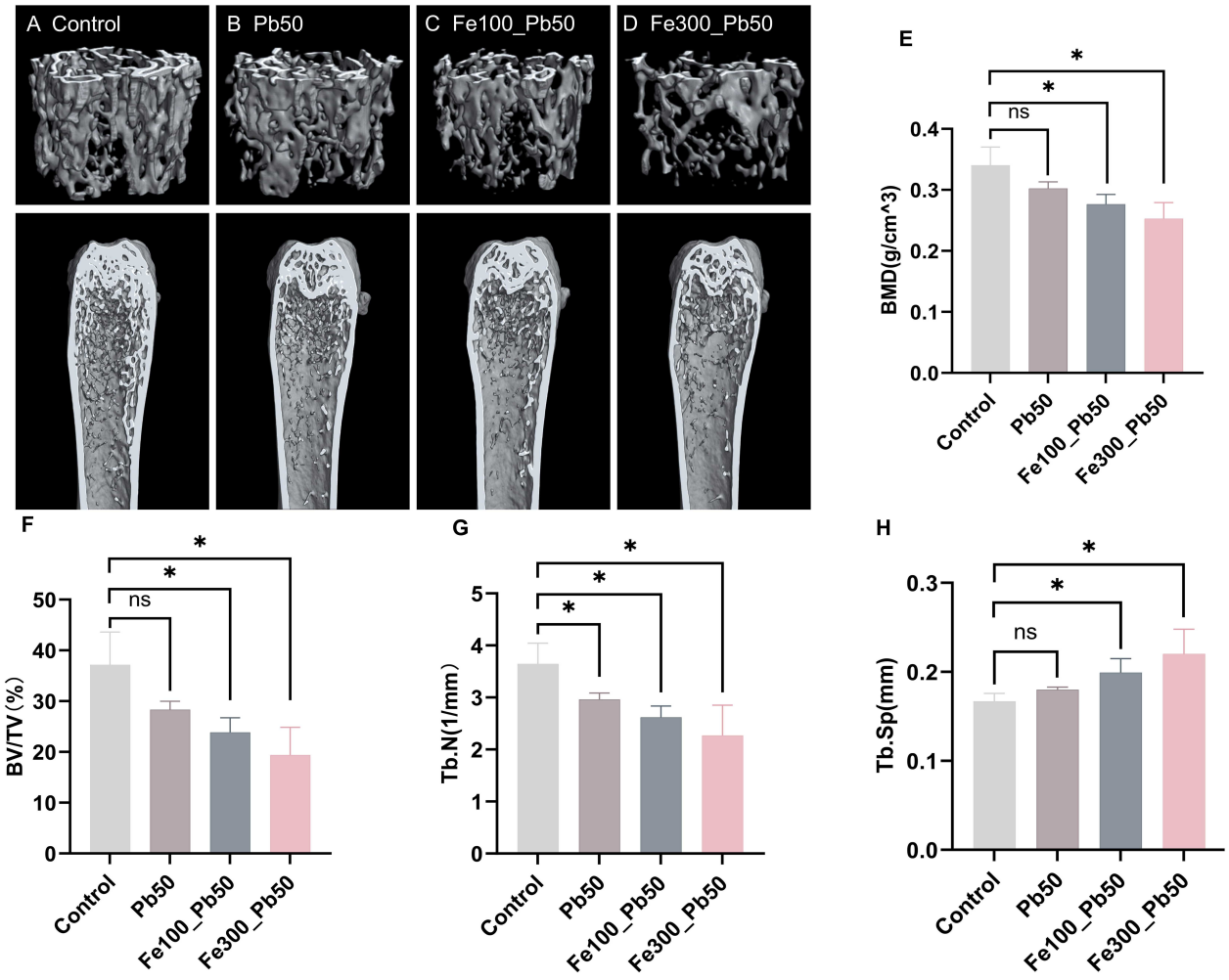

Fig. 3. Effects of combined iron–lead exposure on bone microarchitecture in mouse femurs. (A–D) Representative micro-CT reconstructions of femurs across different groups. (E–H) Quantitative analysis of BMD, BV/TV, Tb.N, and Tb.Sp in femurs. *$p < 0.05$, with no significant differences between control and Pb50 groups for (E,F,H) (ns). Data are presented as the mean ± standard deviation (SD).

metabolites were 2-nitrophenol, I-AB-MECA, and 5′-S-Methyl-5′-thioadenosine (**Supplementary Table 1**), whereas the most downregulated metabolites were N2, N2-dimethylguanosine, 2-methylbutyroylcarnitine, and dodecanoylcarnitine (**Supplementary Table 2**). In the Fe300_Pb50 vs Pb50 comparison, the most significantly upregulated metabolites included 5′-S-Methyl-5′-thioadenosine, monophospho-N-acetylneuraminic acid, and glycyl-L-leucine (**Supplementary Table 3**), while the most downregulated metabolites included glucuronide of $C_8H_{16}O_2$, Tiglic acid, and Methionine sulfone (**Supplementary Table 4**).

3.3.3 Correlation Analysis of Differential Metabolites

Spearman correlation analysis was performed to investigate relationships among metabolites in both the low-dose and high-dose groups, with a focus on significantly altered metabolites. A correlation heatmap (Fig. 6) was generated for the five most upregulated and five most downregulated metabolites among the 35 shared metabolites. Significant positive correlations were observed between glycyl-L-leucine and Ethoxyquin-related metabolites, suggesting potential co-variation across both low- and high-dose groups. Glycyl-L-leucine showed strong positive correlations with multiple metabolites. Significant negative correlations were primarily observed between ethylphosphorothioic acid and tiglic acid, as well as between 5′-S-Methyl-5′-thioadenosine and 2-methylbutyroylcarnitine.

3.3.4 Pathway Enrichment Analysis of Differential Metabolites

Pathway enrichment analysis of differential metabolites was performed using the Kyoto Encyclopedia of Genes and Genomes (KEGG) database. This analysis identified significantly enriched metabolic pathways, providing insight into underlying biological processes. Differential

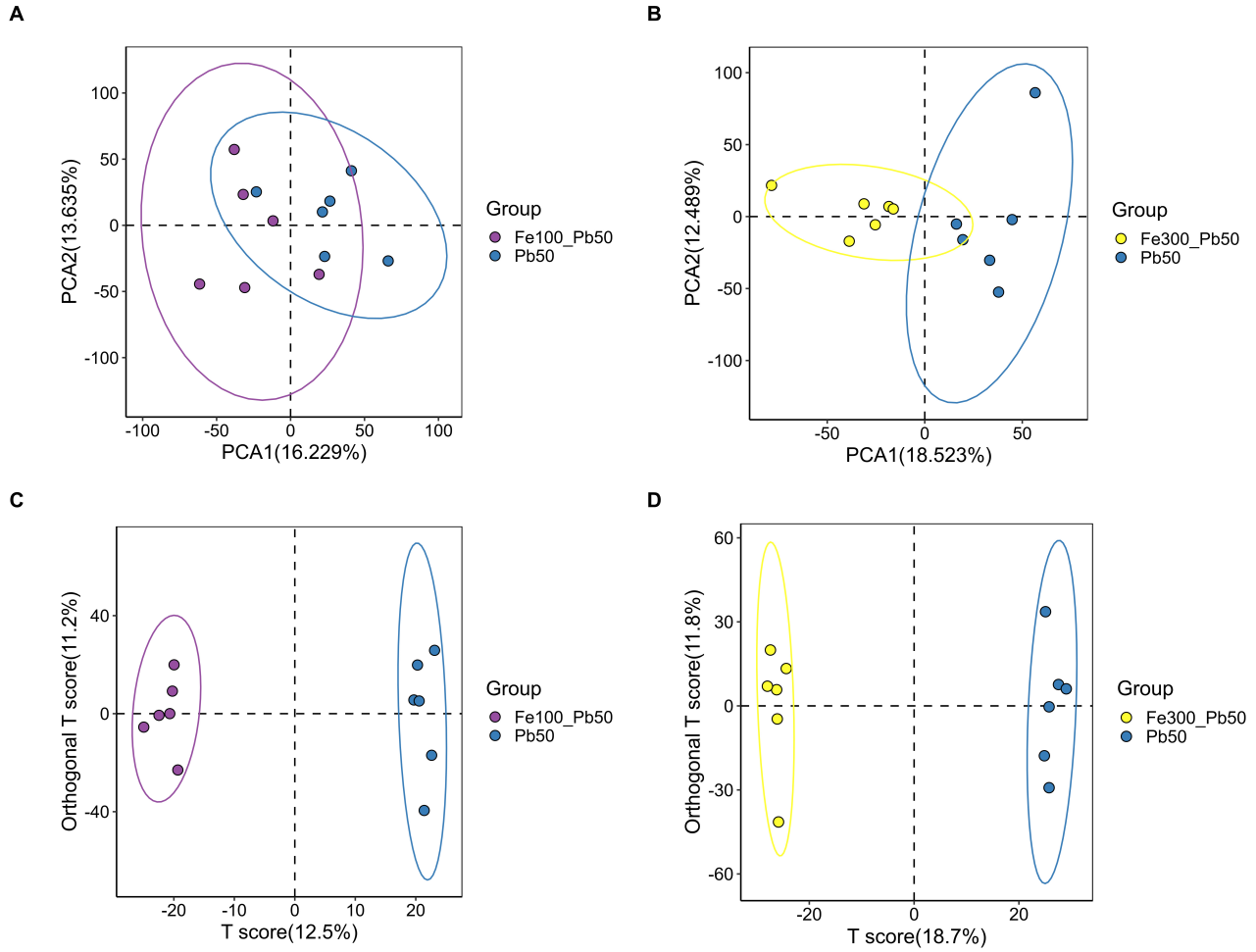

Fig. 4. Multivariate analysis of metabolomic profiles across groups. (A,B) Principal component analysis (PCA) score plots (n = 6 per group). The x-axis represents PC1 and the y-axis represents PC2. Values in parentheses indicate the percentage of variance explained. (C,D) Orthogonal partial least squares discriminant analysis (OPLS-DA) score plots. The x-axis (T score [1]) represents the predictive component, and the y-axis (orthogonal T score [1]) represents the orthogonal component. Each point represents a sample, with different colors indicating different groups; ellipses denote the 95% confidence intervals.

metabolites were considered significantly enriched at $p < 0.05$. Bubble plots were used to display the top 10 enriched pathways ranked by p values. In the Fe100_Pb50 vs Pb50 comparison, "Regulation of lipolysis in adipocytes" showed the highest enrichment ratio, with a RichFactor of approximately 0.1429. The pathways with the highest numbers of differential metabolites were "Biosynthesis of amino acids" and "ABC transporters", each containing five metabolites (Fig. 7A).

In the Fe300_Pb50 vs Pb50 comparison, distinct pathway enrichment patterns were observed. "Protein digestion and absorption" showed the highest enrichment ratio (RichFactor = 0.2766), followed by "Mineral absorption" (RichFactor = 0.2759); however, this finding does not directly reflect transporter protein activity. "Biosynthesis of amino acids" contained the largest number of differential metabolites (n = 16) (Fig. 7B). Both groups showed enrichment in pathways including "Biosynthesis of amino acids", "ABC transporters", "Protein digestion and absorption", and "Central carbon metabolism in cancer".

4. Discussion

In this study, we systematically investigated the effects of iron overload on bone metabolism under fixed lead exposure in a mouse model. By integrating ICP-MS, micro-CT, and bone tissue-specific untargeted metabolomics, we demonstrated that increasing iron burden did not significantly alter lead deposition in bone but markedly disrupted mineral homeostasis and metabolic profiles. Notably, iron overload exacerbated the depletion of essential trace elements, including calcium, zinc, magnesium, and vanadium, and induced extensive metabolic reprogramming in bone tissue. These findings indicate that iron overload exacerbates bone metabolic disorders in the context of lead exposure, highlighting the complexity of mixed-metal toxicity in skeletal health. Importantly, this study demonstrates that

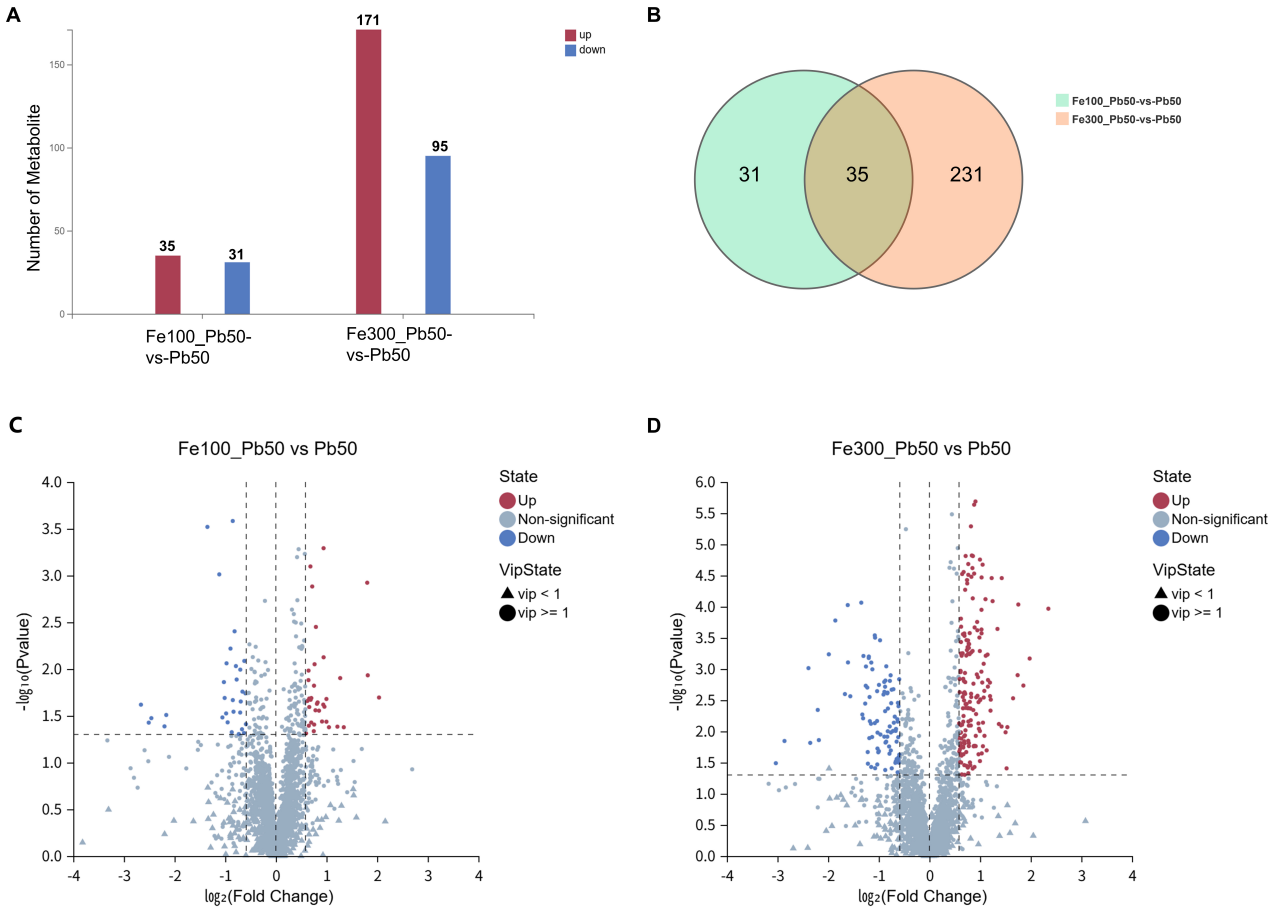

Fig. 5. Differential metabolite analysis in mouse femurs. (A) Differential metabolite profiles across groups. The x-axis represents comparison groups, and the y-axis indicates the number of metabolites. Red and blue denote significantly upregulated and downregulated metabolites, respectively. (B) Venn diagram showing shared and unique differential metabolites between the Fe100_Pb50 vs Pb50 (green) and Fe300_Pb50 vs Pb50 (orange) groups. (C,D) Volcano plots of differential metabolites for the Fe100_Pb50 vs Pb50 and Fe300_Pb50 vs Pb50 comparisons. The x-axis represents $\log_2$ fold change, and the y-axis represents $-\log_{10}$ p value. Red and blue indicate significantly upregulated and downregulated metabolites, respectively; gray indicates non-significant metabolites. Circles and triangles denote metabolites with Variable Importance in Projection (VIP) $\geq$1 and <1, respectively.

iron overload exacerbates bone metabolic dysfunction under fixed lead exposure conditions, independent of changes in skeletal lead accumulation.

Previous histomorphometric studies have shown that external stimuli, such as electrical or ultrasonic stimulation, can significantly alter trabecular bone structure, osteoid formation, and bone remodeling dynamics [26]. Together with the micro-CT findings of this study, as well as the observed mineral imbalance and metabolic reprogramming, these results suggest that metabolic abnormalities are closely associated with structural changes in bone. These alterations may collectively contribute to bone metabolic disorders at both structural and functional levels.

These structural changes may be linked to altered metal transport and trace element homeostasis. Previous studies have suggested that iron and lead may share common transport and regulatory mechanisms, including divalent metal transporter 1 (DMT1) and ATP-binding cassette (ABC) transporters, which may underlie their interactions in bone tissue [27,28,29]. Although the involvement of DMT1 and ABC transporters has been suggested in previous studies, direct experimental evidence in bone tissue remains limited and warrants further investigation. In addition, other metal transporters, such as ZIP/ZnT zinc transporters and the iron exporter ferroportin (FPN), have been reported to play important roles in maintaining trace element homeostasis [23]. These transporters mediate the uptake, transport, and distribution of various divalent metal ions. Excess iron may competitively occupy shared transport pathways, particularly DMT1 [30]. Iron overload may also disrupt zinc homeostasis by interfering with ZIP/ZnT transporters. Furthermore, iron overload may alter systemic metal distribution by modulating ferroportin-mediated iron export [31,32]. Collectively, these processes may disrupt

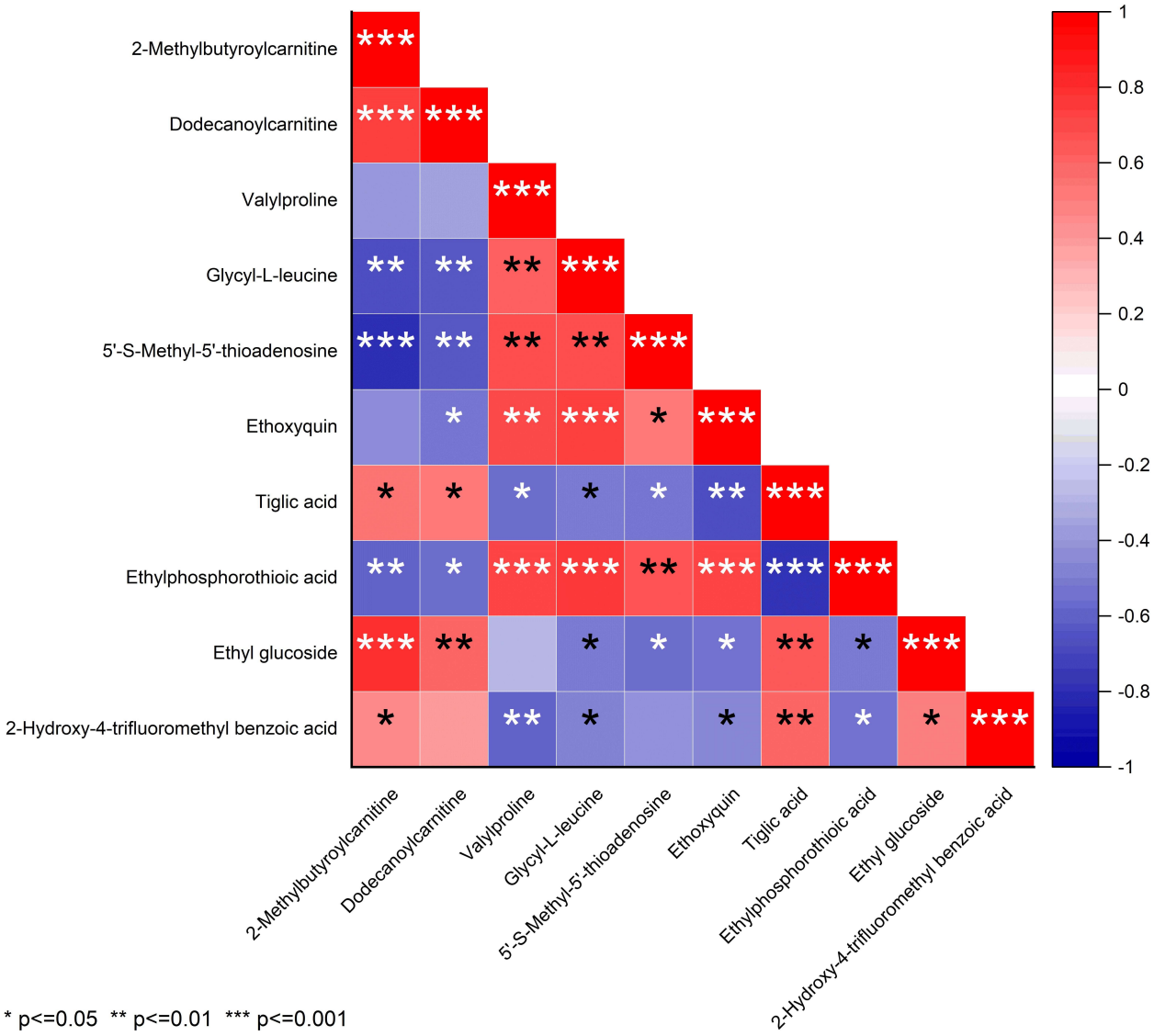

Fig. 6. Heatmap of Spearman correlation analysis results. Colors indicate the strength of correlation, with red representing positive correlations and blue representing negative correlations. Color intensity reflects the absolute value of the correlation coefficient, with deeper colors indicating stronger associations between metabolites. (*$p < 0.05$; **$p < 0.01$; ***$p < 0.001$).

the uptake and distribution of essential minerals required for bone mineralization. The observed negative correlations between iron and calcium, zinc, magnesium, and vanadium suggest that iron overload may disrupt the tightly regulated trace element network in bone. Calcium is a major component of hydroxyapatite and is essential for bone mineralization, whereas zinc plays a critical role in osteoblast activity and collagen synthesis. Magnesium contributes to crystal formation and structural stability, and vanadium has been implicated in the regulation of bone growth and mineral metabolism. Disruption of these elements may impair osteoblast function, collagen production, and hydroxyapatite formation [33,34]. This mineral imbalance may represent a key mechanism by which iron overload and lead exposure synergistically exacerbate bone toxicity [35,36].

In addition to mineral imbalance, metabolic reprogramming may also contribute to bone dysfunction. Bone tissue–specific metabolomics revealed pronounced alterations in pathways related to amino acid metabolism, nucleotide metabolism, and mineral transport. Functionally, these alterations can be categorized into three main aspects: protein synthesis, energy metabolism, and mineral homeostasis. Alterations in amino acid biosynthesis and aminoacyl-tRNA biosynthesis suggest impaired protein synthesis, particularly affecting collagen production and osteoblast activity, which are essential for bone matrix formation [37,38]. These disruptions further indicate impaired bone matrix synthesis under iron–lead co-exposure [39]. Alterations in nucleotide metabolism may reflect disturbances in cellular energy balance and proliferation, both

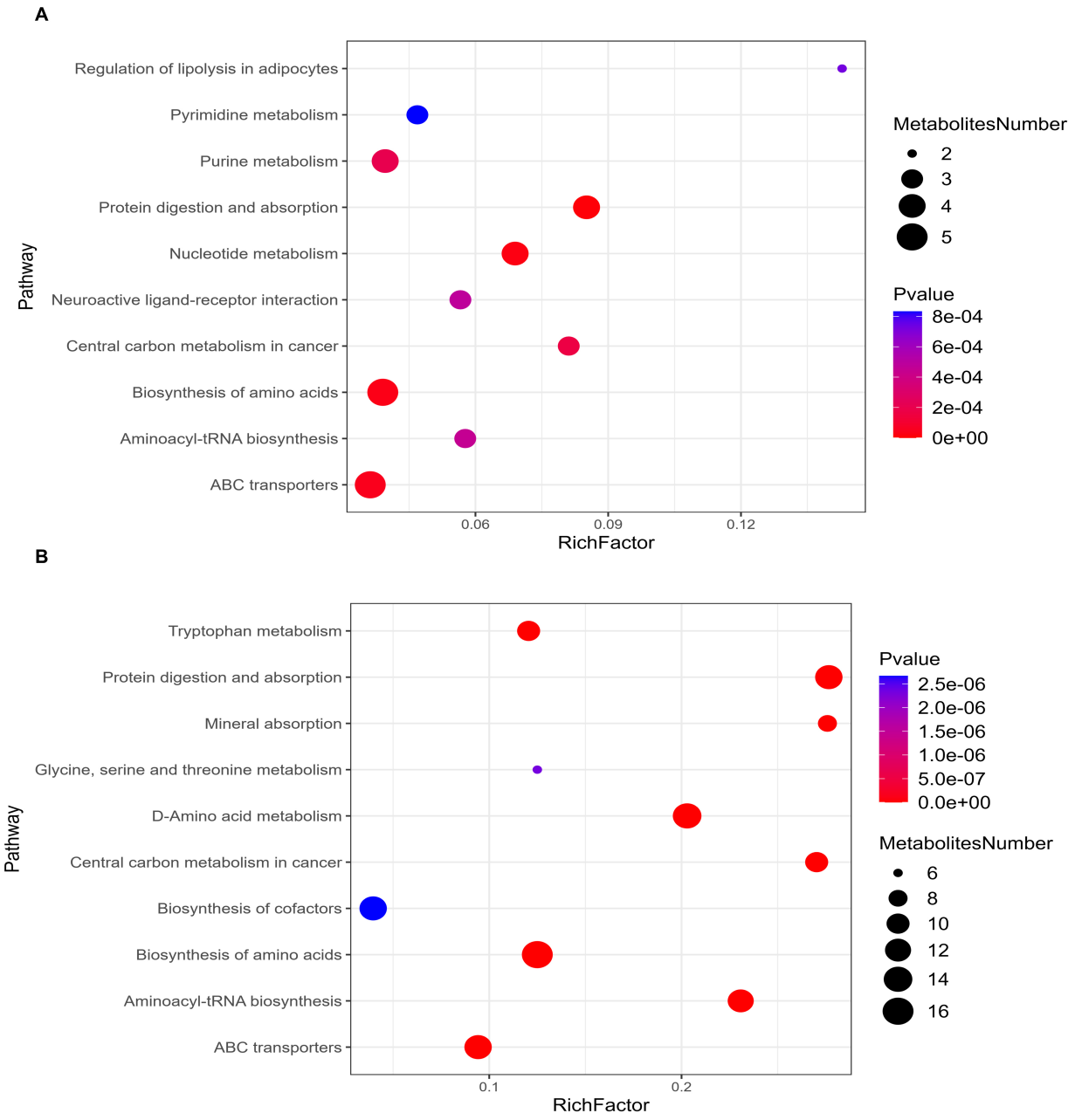

Fig. 7. Kyoto Encyclopedia of Genes and Genomes (KEGG) pathway enrichment analysis of differential metabolites. (A) Metabolic pathway analysis of the Fe100_Pb50 vs Pb50 group. (B) Metabolic pathway analysis of the Fe300_Pb50 vs Pb50 group. The x-axis represents the enrichment factor (RichFactor), with larger values indicating a higher proportion of differential metabolites in the pathway. Dot size represents the number of differential metabolites annotated to each pathway, while color indicates statistical significance; red represents lower *p* values (more significant), and blue represents higher *p* values (less significant).

of which are critical for active bone remodeling. Enrichment of ABC transporter–related pathways suggests impaired mineral transport and homeostasis, further contributing to bone metabolic dysfunction [40].

Distinct dose-dependent metabolic patterns were observed between low- and high-dose iron exposure. At the functional level, low-dose iron exposure was primarily associated with alterations in lipid and nucleotide metabolism, suggesting an early adaptive response involving membrane remodeling and energy regulation [41,42,43,44]. In contrast, high-dose iron exposure predominantly affected pathways related to mineral absorption and cofactor biosynthesis, suggesting more severe disruption of mineral homeostasis and enzymatic processes required for bone metabolism [45,46].

Collectively, these findings suggest that increasing iron burden shifts bone metabolism from an adaptive state toward functional impairment in protein synthesis, energy metabolism, and mineral regulation, ultimately contributing to structural and metabolic bone damage.

5. Limitations

Although rigorous quality control and multivariate modeling were applied to enhance data reliability, potential experimental bias and inter-individual variability in metal exposure cannot be entirely excluded [47,48]. In addition, as this study was conducted in a mouse model, species-specific differences in metal metabolism may limit the direct extrapolation of these findings to humans. From a study design perspective, blank control groups were not included in the ICP-MS and untargeted metabolomics analyses, and an iron-only exposure group was not established. Therefore, it is difficult to distinguish baseline changes from the independent effects of iron overload and its interaction with lead exposure.

Lead was administered via oral gavage, whereas iron dextran was delivered via intraperitoneal injection; these differences in administration routes may introduce confounding effects on metal absorption, distribution, and metabolism. Conclusions regarding bone metabolic dysfunction also lack comprehensive functional validation, such as histopathological assessment and bone metabolism markers. In addition, the metabolomics findings are primarily exploratory and require further validation through targeted LC-MS/MS analysis and functional experiments to elucidate the underlying molecular mechanisms. This study also lacks *in vitro* or molecular-level mechanistic validation; therefore, the conclusion that iron overload aggravates bone dysfunction requires further confirmation.

6. Conclusions

In summary, this study demonstrates that the interaction between iron overload and lead exposure disrupts bone metabolism. Notably, increased iron levels did not significantly affect lead deposition in the femur but were associated with more pronounced mineral imbalance and skeletal alterations under lead exposure. These effects were characterized by alterations in bone microarchitecture and disruptions in essential mineral levels. Metabolomic analysis further indicated that co-exposure to iron and lead may contribute to bone metabolic imbalance through pathways involving ABC transporters, protein digestion and absorption, and amino acid biosynthesis. Collectively, these findings provide new insights into the combined effects of iron and lead on bone metabolism and may help inform strategies for the prevention and treatment of osteoporosis.

Availability of Data and Materials

All data generated or analyzed during this study are included in this published article and its supplementary information files. The datasets used in this study are available upon reasonable request from the corresponding author.

Author Contributions

YY, TC and DY designed the research study. YY, HM and LL performed the research. YY and TG analyzed the data and wrote the manuscript. All authors contributed to critical revision of the manuscript for important intellectual content. All authors read and approved the final manuscript. All authors have participated sufficiently in the work and agreed to be accountable for all aspects of the work.

Ethics Approval and Consent to Participate

All animal experiments were reviewed and approved by the Ethics Committee of Anhui Medical University (Approval No. 2024-2251). All experimental procedures were conducted in strict accordance with institutional guidelines and national regulations governing the care and use of laboratory animals, and followed the ARRIVE guidelines. Every effort was made to minimize animal suffering and to reduce the number of animals used.

Acknowledgment

Graphic abstract was created with https://BioRender.com. Yang, Y. (2026) https://BioRender.com/r9n8yai.

Funding

This work was supported by the Higher Education Scientific Research Project of the Anhui Provincial Department of Education, China (Grant No. 2024AH050545).

Conflicts of Interest

The authors declare no conflicts of interest.

Supplementary Material

Supplementary material associated with this article can be found, in the online version, at https://doi.org/10.31083/FBL50432.

References

[1] Wang J, Shu B, Tang DZ, Li CG, Xie XW, Jiang LJ, et al. The prevalence of osteoporosis in China, a community based cohort study of osteoporosis. Frontiers in Public Health. 2023; 11: 1084005. https://doi.org/10.3389/fpubh.2023.1084005

[2] LeBoff MS, Greenspan SL, Insogna KL, Lewiecki EM, Saag KG, Singer AJ, et al. The clinician's guide to prevention and treatment of osteoporosis. Osteoporosis International : a Journal Established as Result of Cooperation between the European Foundation for Osteoporosis and the National Osteoporosis Foundation of the USA. 2022; 33: 2049–2102. https://doi.org/10.1007/s00198-021-05900-y

[3] Ebeling PR, Nguyen HH, Aleksova J, Vincent AJ, Wong P, Milat F. Secondary Osteoporosis. Endocrine Reviews. 2022; 43: 240–313. https://doi.org/10.1210/endrev/bnab028
[4] Compston JE, McClung MR, Leslie WD. Osteoporosis. Lancet (London, England). 2019; 393: 364–376. https://doi.org/10.1016/S0140-6736(18)32112-3
[5] Wang S, Li Q, Gao Y, Zhou Z, Li Z. Influences of lead exposure on its accumulation in organs, meat, eggs and bone during laying period of hens. Poultry Science. 2021; 100: 101249. https://doi.org/10.1016/j.psj.2021.101249
[6] Liu S, Wang H, Cao Y, Lu L, Wu Y, Lian F, et al. The association between low-concentration heavy metal exposure and chronic kidney disease risk through α-klotho. Scientific Reports. 2025; 15: 11320. https://doi.org/10.1038/s41598-025-96016-4
[7] Zhang S, Deng Z, Yin X, Fang H, Song G, Liu Y, et al. Bioaccessibility of lead and cadmium in soils around typical lead-acid power plants and their effect on gut microorganisms. Environmental Geochemistry and Health. 2024; 46: 107. https://doi.org/10.1007/s10653-023-01840-0
[8] Wei M, Huang Q, Dai Y, Zhou H, Cui Y, Song W, et al. Manganese, iron, copper, and selenium co-exposure and osteoporosis risk in Chinese adults. Journal of Trace Elements in Medicine and Biology : Organ of the Society for Minerals and Trace Elements (GMS). 2022; 72: 126989. https://doi.org/10.1016/j.jtemb.2022.126989
[9] Zhang J, Hu W, Ding C, Yao G, Zhao H, Wu S. Deferoxamine inhibits iron-uptake stimulated osteoclast differentiation by suppressing electron transport chain and MAPKs signaling. Toxicology Letters. 2019; 313: 50–59. https://doi.org/10.1016/j.toxlet.2019.06.007
[10] Li C, Qu M, Tian X, Zhuang W, Zhu M, Lv S, et al. Epidemiological and transcriptome data identify association between iron overload and metabolic dysfunction-associated steatotic liver disease and hepatic fibrosis. Nutrition Research (New York, N.Y.). 2024; 131: 121–134. https://doi.org/10.1016/j.nutres.2024.09.011
[11] Snega Priya P, Pratiksha Nandhini P, Arockiaraj J. A comprehensive review on environmental pollutants and osteoporosis: Insights into molecular pathways. Environmental Research. 2023; 237: 117103. https://doi.org/10.1016/j.envres.2023.117103
[12] Yang Y, Yuan S, Gong T, Zhang J, Ma H, Yu D, et al. Metallic Contaminants and Osteoporosis: a Review of the Gut-Bone Axis. Biological Trace Element Research. 2025. https://doi.org/10.1007/s12011-025-04913-6
[13] Chang J, Kueon C, Kim J. Influence of lead on repetitive behavior and dopamine metabolism in a mouse model of iron overload. Toxicological Research. 2014; 30: 267–276. https://doi.org/10.5487/TR.2014.30.4.267
[14] Zhu G, Fan G, Feng C, Li Y, Chen Y, Zhou F, et al. The effect of lead exposure on brain iron homeostasis and the expression of DMT1/FP1 in the brain in developing and aged rats. Toxicology Letters. 2013; 216: 108–123. https://doi.org/10.1016/j.toxlet.2012.11.024
[15] Zhou F, Chen Y, Fan G, Feng C, Du G, Zhu G, et al. Lead-induced iron overload and attenuated effects of ferroportin 1 overexpression in PC12 cells. Toxicology in Vitro : an International Journal Published in Association with BIBRA. 2014; 28: 1339–1348. https://doi.org/10.1016/j.tiv.2014.07.005
[16] Zhu H, Shen F, Liao T, Qian H, Liu Y. Sporidiobolus pararoseus polysaccharides relieve rheumatoid arthritis by regulating arachidonic acid metabolism and bone remodeling signaling pathway. International Journal of Biological Macromolecules. 2024; 281: 136272. https://doi.org/10.1016/j.ijbiomac.2024.136272
[17] Nelea V, Ittah E, McKee MD, Reznikov N. Bone mineral tessellation: Atomic force microscopy of the volume-filling mineralization pattern in hydrated and dehydrated states. Acta Biomaterialia. 2025; 200: 251–264. https://doi.org/10.1016/j.actbio.2025.05.016
[18] He Y, Su J, Gao H, Li J, Feng Z, Yin Y. Untargeted Metabolomics Reveals the Function of GPRC6A in Amino Acid and Lipid Metabolism in Mice. Metabolites. 2022; 12: 776. https://doi.org/10.3390/metabo12090776
[19] Kang H, Strong AL, Sun Y, Guo L, Juan C, Bancroft AC, et al. The HIF-1α/PLOD2 axis integrates extracellular matrix organization and cell metabolism leading to aberrant musculoskeletal repair. Bone Research. 2024; 12: 17. https://doi.org/10.1038/s41413-024-00320-0
[20] Fan J, Jahed V, Klavins K. Metabolomics in Bone Research. Metabolites. 2021; 11: 434. https://doi.org/10.3390/metabo11070434
[21] Lv H, Jiang F, Guan D, Lu C, Guo B, Chan C, et al. Metabolomics and Its Application in the Development of Discovering Biomarkers for Osteoporosis Research. International Journal of Molecular Sciences. 2016; 17: 2018. https://doi.org/10.3390/ijms17122018
[22] Zhang J, Ma H, Yang Y, Liu L, Luo D, Yu D, et al. Iron-lead mixed exposure causes bone damage in mice: A multi-omics analysis. Ecotoxicology and Environmental Safety. 2025; 292: 117967. https://doi.org/10.1016/j.ecoenv.2025.117967
[23] Kondaiah P, Yaduvanshi PS, Sharp PA, Pullakhandam R. Iron and Zinc Homeostasis and Interactions: Does Enteric Zinc Excretion Cross-Talk with Intestinal Iron Absorption? Nutrients. 2019; 11: 1885. https://doi.org/10.3390/nu11081885
[24] Ravet K, Pilon M. Copper and iron homeostasis in plants: the challenges of oxidative stress. Antioxidants & Redox Signaling. 2013; 19: 919–932. https://doi.org/10.1089/ars.2012.5084
[25] Gao Z, Chen Z, Xiong Z, Liu X. Ferroptosis - A new target of osteoporosis. Experimental Gerontology. 2022; 165: 111836. https://doi.org/10.1016/j.exger.2022.111836
[26] Coman M, Hîncu M, Surlin P, Mateescu G, Nechita A, Banu M. Comparative histomorphometric study of bone tissue synthesized after electric and ultrasound stimulation. Romanian Journal of Morphology and Embryology = Revue Roumaine De Morphologie et Embryologie. 2011; 52: 455–458.
[27] Mani MS, Dsouza VL, Dsouza HS. Evaluation of divalent metal transporter 1 (DMT1) (rs224589) polymorphism on blood lead levels of occupationally exposed individuals. Toxicology Letters. 2021; 353: 13–19. https://doi.org/10.1016/j.toxlet.2021.10.002
[28] Cheli VT, Santiago González DA, Marziali LN, Zamora NN, Guitart ME, Spreuer V, et al. The Divalent Metal Transporter 1 (DMT1) Is Required for Iron Uptake and Normal Development of Oligodendrocyte Progenitor Cells. The Journal of Neuroscience : the Official Journal of the Society for Neuroscience. 2018; 38: 9142–9159. https://doi.org/10.1523/JNEUROSCI.1447-18.2018
[29] Gaál A, Torma L, Bakos É, Német K, Kregsamer P, Streli C, et al. ABCC1 promotes GSH-dependent iron transport and resistance to Fe(II) and Cu(II) chelators. Biometals : an International Journal on the Role of Metal Ions in Biology, Biochemistry, and Medicine. 2025; 38: 1881–1895. https://doi.org/10.1007/s10534-025-00736-z
[30] Liziczai M, Fuchs A, Manatschal C, Dutzler R. Structural basis for metal ion transport by the human SLC11 proteins DMT1 and NRAMP1. Nature Communications. 2025; 16: 761. https://doi.org/10.1038/s41467-024-54705-0
[31] Illing AC, Shawki A, Cunningham CL, Mackenzie B. Substrate profile and metal-ion selectivity of human divalent metal-ion transporter-1. The Journal of Biological Chemistry. 2012; 287: 30485–30496. https://doi.org/10.1074/jbc.M112.364208

[32] Rolić T, Yazdani M, Mandić S, Distante S. Iron Metabolism, Calcium, Magnesium and Trace Elements: A Review. Biological Trace Element Research. 2025; 203: 2216–2225. https://doi.org/10.1007/s12011-024-04289-z

[33] Cheng Q, Zhang X, Jiang J, Zhao G, Wang Y, Xu Y, et al. Postmenopausal Iron Overload Exacerbated Bone Loss by Promoting the Degradation of Type I Collagen. BioMed Research International. 2017; 2017: 1345193. https://doi.org/10.1155/2017/1345193

[34] Syn NL, Lee PC, Kovalik JP, Tham KW, Ong HS, Chan WH, et al. Associations of Bariatric Interventions With Micronutrient and Endocrine Disturbances. JAMA Network Open. 2020; 3: e205123. https://doi.org/10.1001/jamanetworkopen.2020.5123

[35] Chen Y, Zhu M, Sheng S, Yang H, Zhang Q, Chen X, et al. Biomimetic Extracellular Vesicles Containing Biominerals for Targeted Osteoporosis Therapy. ACS Applied Materials & Interfaces. 2025; 17: 5823–5840. https://doi.org/10.1021/acsami.4c17238

[36] Hayann L, Socorro M, Vilela AFL, Cominal JG, Andrilli LHDS, Ciancaglini P, et al. Strontium Changes Lipid Profile, Release, and Function of Matrix Vesicles Produced by Mineralization-Competent Cells. Frontiers in Bioscience (Landmark edition). 2025; 30: 47664. https://doi.org/10.31083/FBL47664

[37] Si Z, Zhou S, Shen Z, Luan F. High-Throughput Metabolomics Discovers Metabolic Biomarkers and Pathways to Evaluating the Efficacy and Exploring Potential Mechanisms of Osthole Against Osteoporosis Based on UPLC/Q-TOF-MS Coupled With Multivariate Data Analysis. Frontiers in Pharmacology. 2020; 11: 741. https://doi.org/10.3389/fphar.2020.00741

[38] Ahn J, Son MK, Jung KH, Kim K, Kim GJ, Lee SH, et al. Aminoacyl-tRNA synthetase interacting multi-functional protein 1 attenuates liver fibrosis by inhibiting TGFβ signaling. International Journal of Oncology. 2016; 48: 747–755. https://doi.org/10.3892/ijo.2015.3303

[39] Liu S, Zheng Y, Ma Y, Sarwar A, Zhao X, Luo T, et al. Evaluation and Proteomic Analysis of Lead Adsorption by Lactic Acid Bacteria. International Journal of Molecular Sciences. 2019; 20: 5540. https://doi.org/10.3390/ijms20225540

[40] Guo Z, Yuan X, Li L, Zeng M, Yang J, Tang H, et al. Genome-Wide Analysis of the ATP-Binding Cassette (ABC) Transporter Family in Zea mays L. and Its Response to Heavy Metal Stresses. International Journal of Molecular Sciences. 2022; 23: 2109. https://doi.org/10.3390/ijms23042109

[41] Rochette L, Dogon G, Rigal E, Zeller M, Cottin Y, Vergely C. Lipid Peroxidation and Iron Metabolism: Two Corner Stones in the Homeostasis Control of Ferroptosis. International Journal of Molecular Sciences. 2022; 24: 449. https://doi.org/10.3390/ijms24010449

[42] Guangji W, Huixin P, Hongfei H, Hai L, Yang F, Shihua L, et al. Aluminum exposure induces ferroptosis in spermatogenic cells of mice through iron overload and lipid peroxidation. Free Radical Biology & Medicine. 2025; 241: 789–806. https://doi.org/10.1016/j.freeradbiomed.2025.09.043

[43] Wang W, Shi F, Cui J, Pang S, Zheng G, Zhang Y. MiR-378a-3p/SLC7A11 regulate ferroptosis in nerve injury induced by lead exposure. Ecotoxicology and Environmental Safety. 2022; 239: 113639. https://doi.org/10.1016/j.ecoenv.2022.113639

[44] Zhang L, Lin Y, Lu AX, Liu JX, Li J, Yan CH. Metabolomics insights into the effects of pre-pregnancy lead exposure on bone metabolism in pregnant rats. Environmental Pollution (Barking, Essex : 1987). 2023; 337: 122468. https://doi.org/10.1016/j.envpol.2023.122468

[45] Du J, Cui H, Zhao Y, Xue H, Chen J. Exposure to air pollution might decrease bone mineral density and increase the prevalence of osteoporosis: a Mendelian randomization study. Osteoporosis International : a Journal Established as Result of Cooperation between the European Foundation for Osteoporosis and the National Osteoporosis Foundation of the USA. 2024; 35: 2215–2223. https://doi.org/10.1007/s00198-024-07249-4

[46] Kupraszewicz E, Brzóska MM. Excessive ethanol consumption under exposure to lead intensifies disorders in bone metabolism: a study in a rat model. Chemico-biological Interactions. 2013; 203: 486–501. https://doi.org/10.1016/j.cbi.2013.01.002

[47] Chen S, Yang JL, Zhang YS, Wang HY, Lin XY, Xue RY, et al. Microplastics affect arsenic bioavailability by altering gut microbiota and metabolites in a mouse model. Environmental Pollution (Barking, Essex : 1987). 2023; 324: 121376. https://doi.org/10.1016/j.envpol.2023.121376

[48] Zhou L, Chen SZ, Li YY, Xue RY, Duan X, Lin XY, et al. Gut Dysbiosis Exacerbates Intestinal Absorption of Cadmium and Arsenic from Cocontaminated Rice in Mice Due to Impaired Intestinal Barrier Functions. Environmental Science & Technology. 2025; 59: 3459–3471. https://doi.org/10.1021/acs.est.5c00817